Superconductivity in rubidium-substituted $Ba_{1-x}Rb_xTi_2Sb_2O$

Fabian von Rohr,[1,2,*] Reinhard Nesper,[2] and Andreas Schilling[1]

[1]*Physik-Institut der Universität Zürich, Winterthurerstrasse 190, CH-8057 Zürich, Switzerland*

[2]*Laboratory of Inorganic Chemistry, ETH Zürich, Wolfgang-Pauli-Strasse 10, CH-8093 Zürich, Switzerland*

(Received 6 November 2013; revised manuscript received 16 January 2014; published 7 March 2014)

We report on the synthesis and the physical properties of $Ba_{1-x}Rb_xTi_2Sb_2O$ ($x \leqslant 0.4$) by x-ray diffraction, superconducting quantum interference device magnetometry, resistivity, and specific-heat measurements. Upon hole doping by substituting Ba with Rb, we find superconductivity with a maximum $T_c = 5.4$ K. Simultaneously, the charge-density-wave transition temperature is strongly reduced from $T_{CDW} \approx 55$ K in the parent compound $BaTi_2Sb_2O$ and seems to be suppressed for $x \geqslant 0.2$. The bulk character of the superconducting state for the optimally doped sample ($x = 0.2$) is confirmed by the occurrence of a well developed discontinuity in the specific heat at T_c, with $\Delta C/T_c \approx 22$ mJ/mol K^2, as well as a large Meissner-shielding fraction of ≈40%. The isotropically averaged lower and upper critical fields of the optimally doped sample ($x = 0.2$) are estimated to $\mu_0 H_{c,1}(0) \approx 3.8$ mT and $\mu_0 H_{c,2}(0) \approx 2.3$ T, respectively, indicating that these compounds are strongly type-II superconductors.

DOI: 10.1103/PhysRevB.89.094505 PACS number(s): 74.62.Bf, 74.25.Op, 74.25.Jb, 74.25.Dw

I. INTRODUCTION

Density waves (DWs) are collective states of broken symmetry that arise from electronic instabilities that are often present in highly anisotropic structures. In some cases they compete with superconductivity, which is an another collective electronic state. The emergence of superconductivity in iron arsenides has attracted great interest in the physical properties of transition metal pnictides in general. In most of these materials, superconductivity occurs in proximity to a spin-density-wave (SDW) transition, and is found to exhibit unconventional properties (see, e.g., Refs. [1,2]). Until now, several systems have been investigated in which superconductivity emerges upon complete or partial suppression of charge-density-wave (CDW) ordering, such as 2H-$NbSe_2$ [3], $Ba_{1-x}K_xBiO_3$ [4,5], and Cu_xTiSe_2 [6]. Likewise, the formation of CDW order has been observed in the normal state of superconducting $YBa_2Cu_3O_{6.67}$ [7].

Most recently, $BaTi_2Sb_2O$ has been found to intrinsically host both distinct states of broken symmetry, showing a CDW ordering transition at $T_{CDW} \approx 55$ K, as well as a transition to superconductivity at $T_c \approx 1$ K [8]. $BaTi_2Sb_2O$ belongs to a large family of stacked, layered titanium oxide pnictide compounds. In these materials the nominal valence of titanium is Ti^{3+} with its $3d$ orbitals singly occupied. In this $3d^1$ configuration, Ti is surrounded octahedrally by O and Sb, forming a Ti_2O square sublattice. From a structural and chemical perspective, these Ti_2O layers can be interpreted as the $3d^1$ anticonfiguration of the $3d^9$ CuO_2 planes in the cuprates.

Upon substitution of barium by sodium or potassium, or of antimony by bismuth or tin, in $BaTi_2Sb_2O$, the CDW ordering temperature T_{CDW} is lowered, while superconductivity reaches a maximum T_c of up to 5.5 K at substitution levels around 15 mol % [9–12]. Detailed nuclear magnetic resonance (NMR) and muon spin resonance (μSR) studies have shown that CDW ordering is most likely competing and coexisting with a conventional superconductor with an s-wave gap [13,14].

In this paper we will show how superconductivity and CDW ordering evolve in $Ba_{1-x}Rb_xTi_2Sb_2O$ as a function of the substitution of barium by rubidium. We will evidence that the CDW ordering transition T_{CDW} is continuously lowered and eventually suppressed with increasing rubidium content, while the transition temperature to superconductivity T_c is increased, reaching a maximum $T_{c,max} = 5.4$ K for $x = 0.2$ (in specific-heat measurements). Our results support that $BaTi_2Sb_2O$ is a versatile model system for the investigation of the competition and coexistence of conventional superconductivity and CDW ordering.

II. EXPERIMENT

Solid-state reactions were employed to synthesize polycrystalline samples of $Ba_{1-x}Rb_xTi_2Sb_2O$ with $x = 0$, 0.02, 0.05, 0.1, 0.15, 0.2, 0.25, 0.3, and 0.4. BaO (99.99%), Rb_2O (95%), Ti (99.99%), TiO_2 (>99%), and Sb (99.999%) were mixed according to the stoichiometric ratio, ground thoroughly, and pressed into pellets of approximately 1 g batches in an argon filled glove box. The pellets were sealed in argon filled (1 atm) niobium ampoules and then sintered at 1000 °C for 72 h. Then the samples were reground under inert atmosphere, repelletized, and sintered again for 24 h at 1000 °C.

X-ray powder diffraction measurements were performed using a Stoe STADIP diffractometer (Cu K_{α_1} radiation, $\lambda = 1.54051$ Å, Ge monochromator). Rietveld refinements and profile fits were performed using the FULLPROF program [15]. The magnetic properties were studied using a Quantum Design magnetic properties measurement system (MPMS XL) equipped with a reciprocating sample option (RSO). The platelike samples were placed in parallel to the external magnetic field in order to minimize demagnetization effects. Specific-heat and resistivity measurements were performed with a Quantum Design physical property measurement system (PPMS). For the resistivity measurements, a standard four-probe technique was employed with 50 μm diameter gold wires attached with silver paint. The applied current for these

*vonrohr@physik.uzh.ch

measurements was $I = 1.5$ mA. Specific-heat measurements were performed with the Quantum Design heat-capacity option using a relaxation technique.

III. RESULTS AND DISCUSSION

In Fig. 1(a) we show the x-ray diffraction pattern at ambient temperature for the sample of nominal composition $Ba_{0.7}Rb_{0.3}Ti_2Sb_2O$ ($x = 0.3$), together with the crystal structure of the compound in the inset. All compounds of the $Ba_{1-x}Rb_xTi_2Sb_2O$ ($x \leqslant 0.4$) solid solution were found to belong to the same crystal structure, which is isopointal to the $CeCr_2Si_2C$-type structure ($P4/mmm$). All compounds of the solid solution are air sensitive and for all investigated dopings the obtained XRD patterns show phase purities larger than $\geqslant$90%. All experimentally observed intensities are in good agreement with the theoretical pattern, indicating the validity of the present structural model. The slight systematic variation of the (111) reflection as a function of rubidium content x is displayed in Fig. 1(b). Within the $Ba_{1-x}Rb_xTi_2Sb_2O$ solid solution ($0 \leqslant x \leqslant 0.4$) the cell parameter varies only slightly, but continuously, with increasing rubidium content. This can

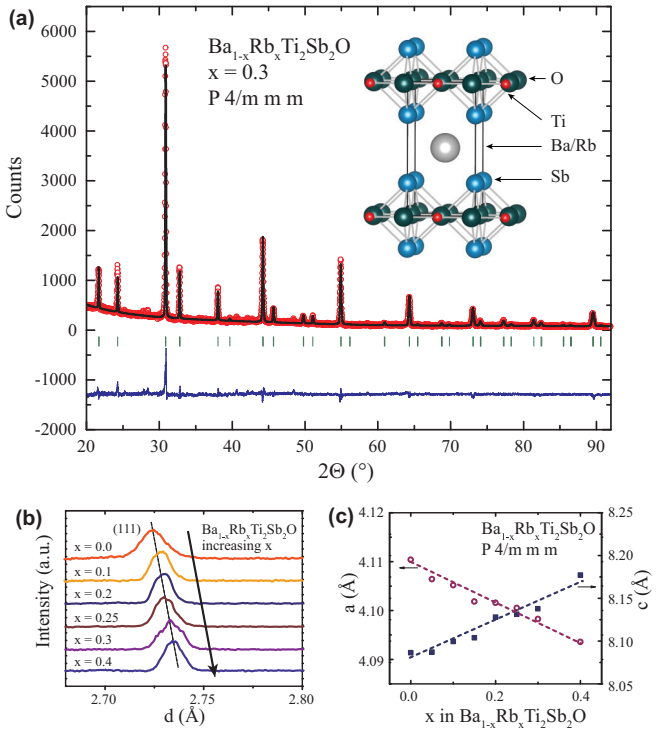

FIG. 1. (Color online) (a) The powder x-ray diffraction (XRD) pattern at ambient temperature for the sample of nominal composition $Ba_{0.7}Rb_{0.3}Ti_2Sb_2O$ ($x = 0.3$). The crystal structure of the compound is shown in the inset. The vertical dark green lines show the theoretical Bragg peak positions for this phase. The blue pattern on the bottom is the difference plot between the theoretical pattern and the observed intensities. (b) Enlarged XRD data around the (111) reflections as functions of increasing x, demonstrating the change in the lattice parameters with Rb content. The dotted line is a guide to the eye. (c) Cell parameters for the different compositions used in this study. The dashed line represents an idealized linear change of the cell parameters.

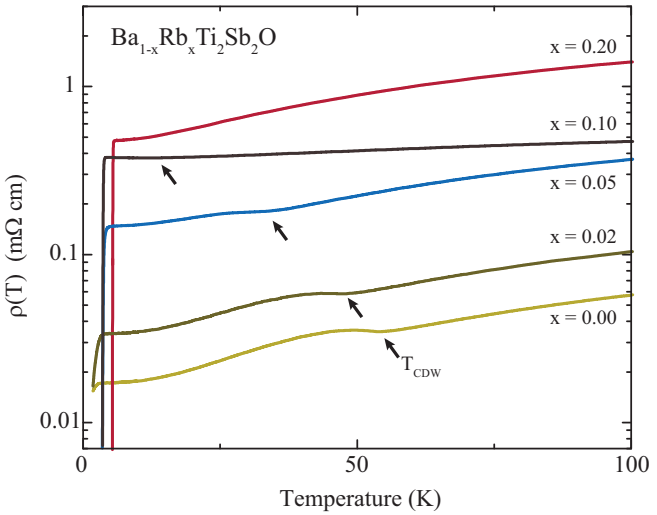

FIG. 2. (Color online) Resistivities of $Ba_{1-x}Rb_xTi_2Sb_2O$ for $x = 0$, 0.02, 0.05, 0.1, and 0.2 in a temperature range between 1.8 and 100 K. The CDW transition manifests itself in a sudden increase of the resistivity for the samples $x = 0$, 0.02, 0.05, and 0.1 (marked with a black arrow). This anomaly is absent for the sample with $x = 0.2$. For increasing rubidium contents x (up to $x = 0.2$), the normal-state resistivities increase, the CDW ordering transition temperatures T_{CDW} decrease, while the critical temperatures T_c increase.

be seen from the small change of a and c, leading to an overall increase of the unit cell volume, obtained from profile fits as shown in Fig. 1(c). The apparent deviation from a linear variation of the cell parameters with x can be attributed to small deviations from the precise stoichiometry, since here we used the nominal x values for all samples. The trend of a contraction of the Ti_2O sheets (decreasing a) and a simultaneous elongation of c with increasing x is in line with observations on potassium-substituted $BaTi_2Sb_2O$ [10]. Our results support the idea that the chemical pressure effect for the superconductivity in these materials is of little importance, whereas the hole doping by the incorporation of Na^+, K^+, and Rb^+, and along with it the variation of the density of states at the Fermi level $D(E_F)$, appears to be of great importance for the occurrence of CDW ordering and/or superconductivity.

The resistivities $\rho(T)$ in a temperature range of $T =$ 1.8–100 K are shown in Fig. 2 for $x = 0$, 0.05, 0.1, and 0.2. All compounds are metals with resistivities ρ(100 K) varying from 0.057 mΩ cm^{-1} for the parent compound to 0.575 mΩ cm^{-1} for $x = 0.2$. The parent compound ($x = 0$) shows a distinct kink in the resistivity at $T_{CDW} = 55$ K, which has earlier been attributed to a CDW transition [14]. This phase transition temperature T_{CDW} is strongly reduced and eventually suppressed with increasing rubidium content. For a relatively small doping of $x = 0.05$, the CDW transition is already lowered to 34 K, whereas the critical temperature is increased by more than 2 K to $T_c = 3.7$ K. Taking the absolute value of the resistivity as a measure for the metallicity of a sample, we can state that the increase of the superconducting transition T_c and the decrease and subsequent suppression of the CDW ordering temperature T_{CDW} go along with a decrease in metallicity. A similar trend for $\rho(T)$ has been reported for Na- and Bi-substituted $BaTi_2Sb_2O$, and it has

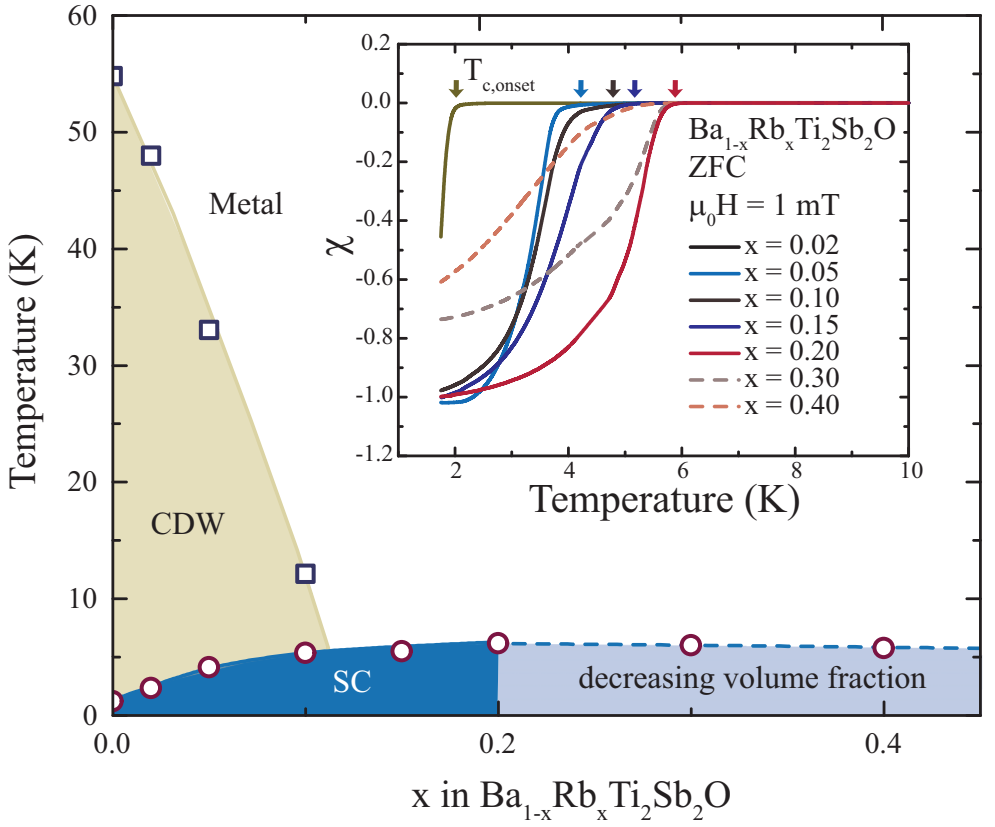

FIG. 3. (Color online) Phase diagram of the electronic properties of $Ba_{1-x}Rb_xTi_2Sb_2O$ derived from resistivity and magnetization measurements (T_c for the parent compound $x = 0$ was taken from Ref. [8]). The inset shows the magnetic susceptibility of $Ba_{1-x}Rb_xTi_2Sb_2O$ for $x = 0.02$, 0.05, 0.1, 0.15, 0.2, 0.3, and 0.4 measured between 1.75 and 10 K in an external magnetic field of $\mu_0 H = 1$ mT in the zero-field-cooled (ZFC) mode. The onsets of the transition to superconductivity $T_{c,onset}$ are marked with arrows. The samples $x = 0.3$ and 0.4 do not display a bulk diamagnetic shielding, and their magnetic susceptibilities are displayed with dashed lines.

been attributed to enhanced impurity scattering or to the proximity to a metal-insulator transition [11,16]. The dc magnetic susceptibility $\chi(T)$ for temperatures from 1.8 to 10 K, measured in a zero-field-cooled (ZFC) mode in an external field of $\mu_0 H = 1$ mT for the samples $x = 0.05$, 0.1, 0.15, 0.2, 0.3, and 0.4, are shown in the inset of Fig. 3. Almost perfect diamagnetic shielding ($\chi = -1$) is observed for the samples $x = 0.05, 0.1, 0.15$, and 0.2 at 1.8 K. The samples with $x = 0.3$ and $x = 0.4$ undergo a transition to a superconducting state at nearly the same temperature as the optimally doped sample with $x = 0.2$. However, their diamagnetic shielding fractions are clearly lowered, leading to the conclusion that doping levels beyond $x > 0.2$ no longer display bulk superconductivity (dashed lines). The onset temperatures of the transition to the superconducting states, $T_{c,onset}$, for the bulk superconducting samples are marked with arrows in the corresponding colors.

In Fig. 3 we summarize the electronic phase diagram of the $Ba_{1-x}Rb_xTi_2Sb_2O$ solid solution, with the superconducting critical temperature T_c for the parent compound $BaTi_2Sb_2O$ taken from Ref. [8]. The critical temperatures T_c used for the phase diagram are the intersections of the slopes of the phase transitions and the normal-state magnetizations. The observed phase diagram for rubidium-substituted $Ba_{1-x}Rb_xTi_2Sb_2O$ is in good agreement with the earlier reported phase diagrams for sodium-, potassium-, and bismuth-substituted $BaTi_2Sb_2O$, with the exception that T_{CDW} decreases more rapidly than in the latter compounds.

The field-dependent resistivity measurements for $x = 0.05$ and optimally doped $x = 0.2$ are shown in Figs. 4(a) and 4(b) for external fields $\mu_0 H \leqslant 3$ T. As expected, the transition temperature T_c is gradually reduced with increasing magnetic fields. We have defined the corresponding upper critical fields H_{c2} using a 50% criterion, i.e., the upper critical field $H_{c2}(T)$ is defined by the temperature T at which 50% of the normal-state resistivity is suppressed [see the dashed lines in Figs. 4(a) and 4(b)]. The resulting temperature dependences of $\mu_0 H_{c2}(T)$ are shown in Fig. 4(c). The extrapolated slopes are for $x = 0.05$, $\frac{dH_{c2}}{dT} = -0.49(6)$ T/K, and for the optimally doped sample with $x = 0.2$, $\frac{dH_{c2}}{dT} = -0.61(3)$ T/K. From these slopes we can evaluate the upper critical fields at zero temperature $\mu_0 H_{c2}(0)$ by applying the Werthamer-Helfand-Hohenberg (WHH) approximation in the dirty limit [17],

$$H_{c2}^{WHH}(0) = -0.69 T_c \left(\frac{dH_{c2}}{dT}\right)_{T=T_c}. \quad (1)$$

The resulting isotropically averaged upper critical fields are $\mu_0 H_{c,2}(0) \approx 1.3$ T for $x = 0.05$, and $\mu_0 H_{c,2}(0) \approx 2.3$ T for $x = 0.2$, respectively.

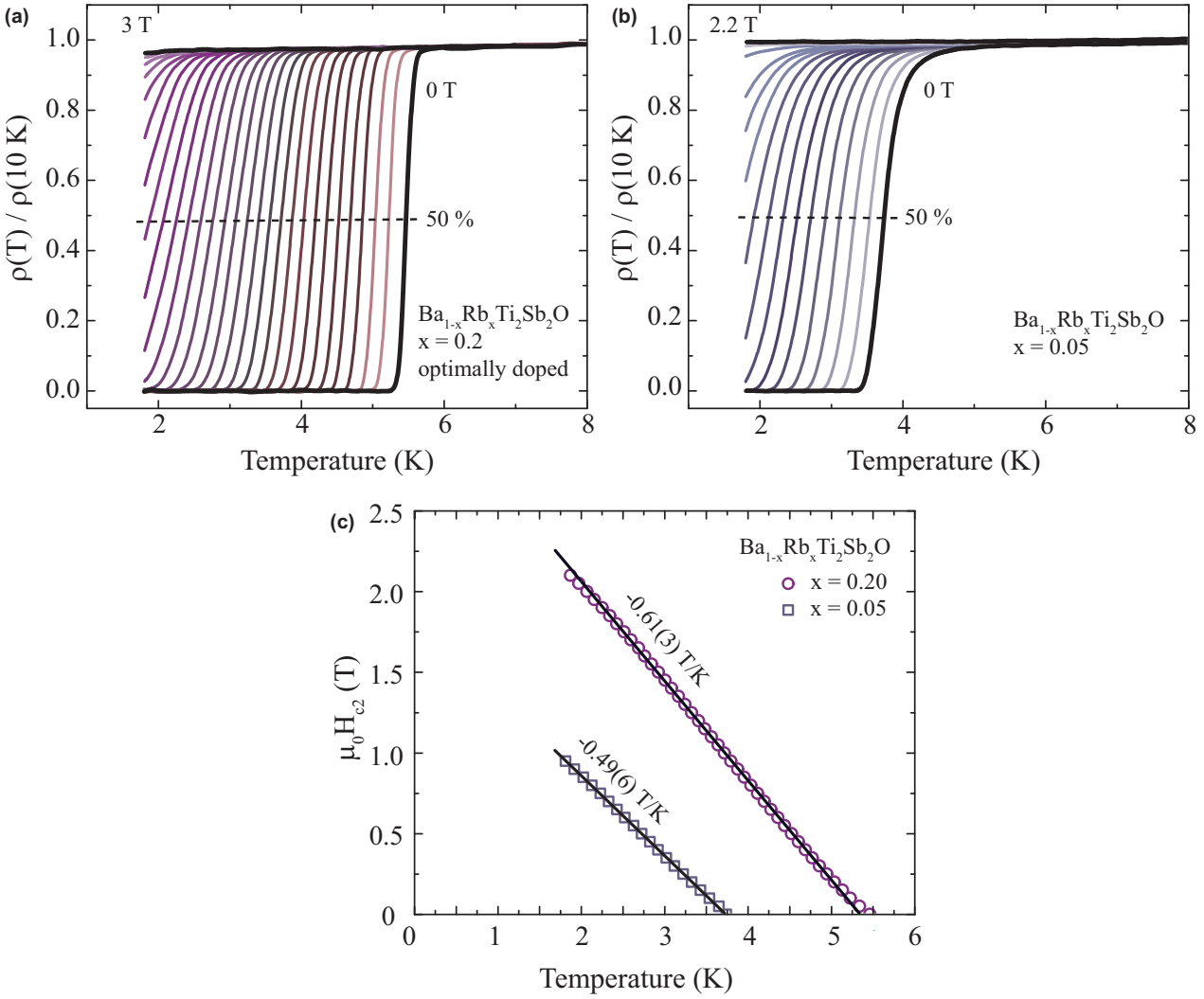

FIG. 4. (Color online) (a) and (b) Normalized resistivity $\rho(T)/\rho(10\ \mathrm{K})$ for the optimally doped sample $x = 0.2$ and $x = 0.05$, respectively. Field-dependent resistivity measurements are shown for magnetic fields between 0 and 3 T, varied by 0.05 T steps, in a temperature range between 1.8 and 8 K. The dashed lines denote the 50% criterion used to determine $H_{c2}(T)$, shown in (c). The solid lines indicate the extrapolated slopes $\frac{dH_{c2}}{dT}$ used for the WHH approximation [Eq. (1)].

According to Ginzburg-Landau theory, the upper critical field at $T = 0$ K, $H_{c2}(0)$, can be used to estimate the coherence length $\xi(0)$ at $T = 0$ K using

$$\mu_0 H_{c2}(0) = \frac{\Phi_0}{2\pi\xi(0)^2}, \tag{2}$$

with $\Phi_0 = h/(2e) \approx 2.0678 \times 10^{-15}$ Wb being the magnetic flux quantum. We obtain isotropically averaged coherence lengths of $\xi(0) = 160$ Å for $x = 0.05$, and $\xi(0) = 120$ Å for the optimally doped sample with $x = 0.2$. Recently, Gooch *et al.* [16] derived, from field-dependent specific-heat measurements for sodium-substituted $Ba_{0.85}Na_{0.15}Ti_2Sb_2O$ with $T_c = 4.2$ K, an upper critical field $H_{c2}(0) = 1.7$ T and a corresponding coherence length $\xi(0) = 140$ Å. Moreover, an upper critical field $H_{c2}(0) = 0.08$ T and a corresponding coherence length $\xi(0) = 640$ Å were reported for the parent compound $BaTi_2Sb_2O$. The coherence lengths $\xi(0)$ and the upper critical fields $H_{c2}(0)$ that we estimated here, for the rubidium-doped $BaTi_2Sb_2O$, are in good agreement with these earlier reported values. The layered structure of these materials implies, as is the case for the cuprates, that the physical properties are highly anisotropic. Therefore, these numbers for H_{c2} and the coherence lengths ξ obtained from polycrystalline samples have to be taken as values appropriately averaged over all crystal directions (see, e.g., Ref. [18]).

In Fig. 5 we show the specific heat of the optimally doped sample ($x = 0.2$) in a C/T vs T representation. The normal-state contribution has been fitted to the data between $T = 6$ and 13 K according to the standard expression

$$\frac{C(T)}{T} = \gamma + \beta T^2, \tag{3}$$

with the Sommerfeld constant γ and $\beta = 12\pi^4 nR/5\Theta_D^3$, where $n = 6$ is the number of atoms per formula unit, $R = 8.13$ J/mol K is the gas constant, and Θ_D is the Debye temperature (dashed line). The obtained value $\gamma \approx 14$ mJ/mol K^2 is in line with corresponding values reported for $BaTi_2Sb_2O$ [8] and $Ba_{0.85}Na_{0.15}Ti_2Sb_2O$ [16], with γ values ranging between

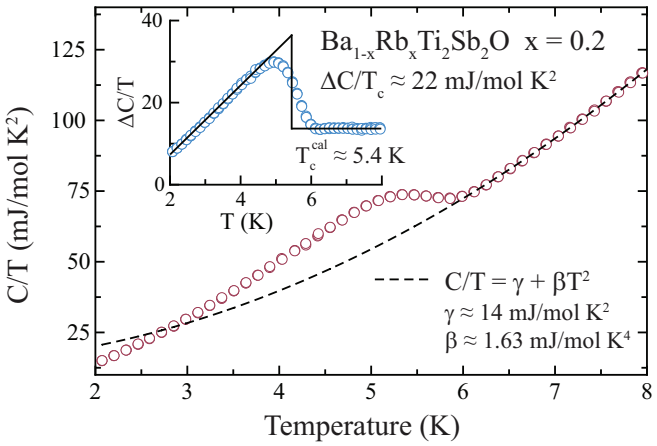

FIG. 5. (Color online) Reduced specific heat C/T vs temperature T of the optimally doped sample ($x = 0.2$), together with an inset showing the same data after subtraction of the normal-state contribution (dashed line in the main panel; see text). The solid lines in the inset represent an entropy-conserving construction to obtain the discontinuity and $\Delta C/T_c$ and T_c^{cal}.

10 and 15 mJ/mol K^2. In the inset of Fig. 5 we show the measured $\Delta C/T$ data, with this normal-state contribution subtracted, together with an entropy-conserving construction to obtain the calorimetrically determined critical temperature T_c^{cal} and the discontinuity $\Delta C/T_c$ at T_c. With $\Delta C/T_c \approx 22$ mJ/mol K^2 at $T_c^{cal} = 5.4$ K we obtain a ratio $\Delta C/\gamma T_c \approx 1.6$, which only slightly exceeds the standard weak-coupling BCS value, $\Delta C/\gamma T_c = 1.43$, again in qualitative agreement with the reported data for $Ba_{0.85}Na_{0.15}Ti_2Sb_2O$ [16]. Here $\beta \approx 1.63$ mJ/mol K^4 corresponds to $\Theta_D \approx 193$ K, which is somewhat smaller than $\Theta_D \approx 210$–239 K, as communicated for $BaTi_2Sb_2O$ and $Ba_{0.85}Na_{0.15}Ti_2Sb_2O$ [8,16].

In the upper inset of Fig. 6 we show the zero-field-cooled (ZFC) and the field-cooled (FC) magnetic susceptibilities for the optimally doped sample $x = 0.2$. The large screening efficiency, as well as a large Meissner shielding of the order of ≈40%, are further indicators of the bulk nature of superconductivity in this compound. The ZFC field dependence of the magnetization $m(H)$ for temperatures between 1.75 and 5 K (in 0.25 K steps) in magnetic fields $\mu_0 H$ between 0 and 15 mT are shown in the main panel of Fig. 6. For comparison, the ideal linear behavior expected in the Meissner state ($\chi = -1$) is also shown (dashed line). It is very difficult to extract precise values for the lower critical field H_{c1} from $m(H)$ measurements, especially for polycrystalline samples. A criterion that is often used in the literature, namely, the identification of H_{c1} as the magnetic field where $m(H)$ first deviates from linearity, does not rely on a sharp feature in the experimental data. A somewhat better criterion was given in Ref. [19] based on Bean's critical-state model [20], although the definition of a linear $m(H)$ regime used in that approach also leaves some

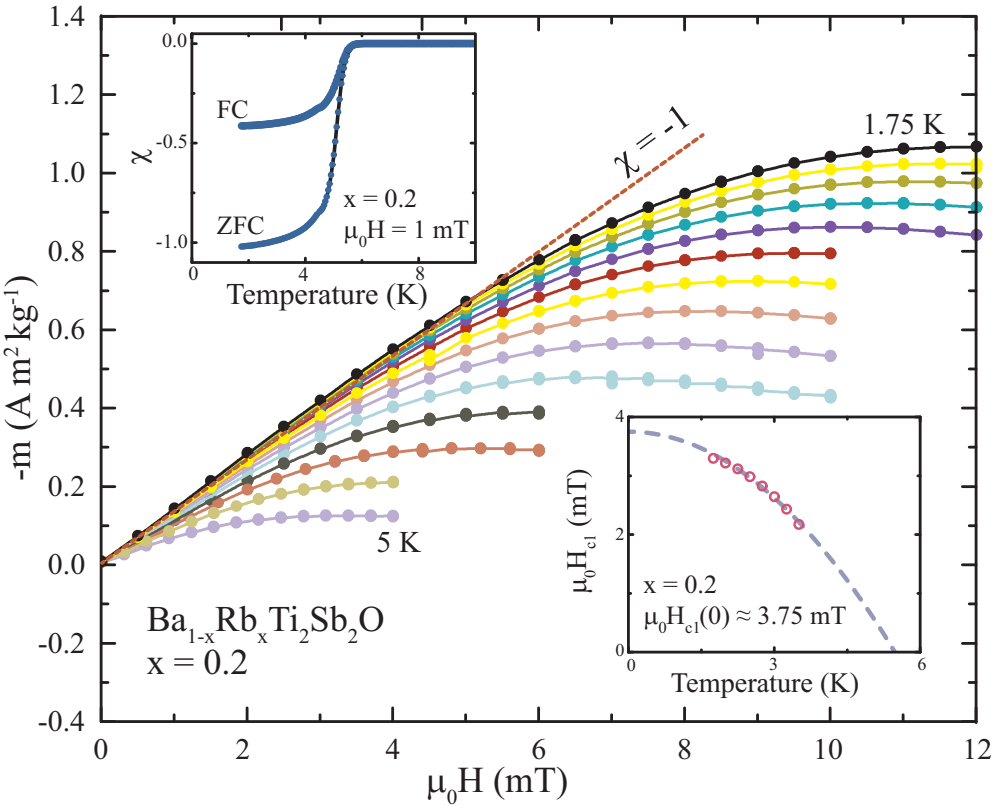

FIG. 6. (Color online) ZFC field dependence of the magnetization $m(H)$ of the optimally doped sample with $x = 0.2$, for temperatures between 1.75 and 5 K (in 0.25 K steps), in magnetic fields $\mu_0 H$ between 0 and 15 mT. The dashed line shows the ideal diamagnetic shielding. Upper inset: ZFC and FC magnetic susceptibility of the sample with $x = 0.2$. Lower inset: The temperature dependence of the lower critical field H_{c1} of the sample with $x = 0.2$ (see text). The dashed line is a fit to Eq. (4) with T_c fixed to 5.4 K.

room for ambiguity. We nevertheless applied the procedure described in Ref. [19] to selected $m(H)$ data for which we could identify a clearly linear $m(H)$ in the limit $H \to 0$ (i.e., for our low-temperature data), and the resulting H_{c1} values are plotted in the lower inset of Fig. 6. A reasonable estimate for $\mu_0 H_{c1}(0)$ can then be obtained by using an empirical formula [21],

$$H_{c1}(T) = H_{c1}(0)[1 - (T/T_c)^2]. \quad (4)$$

With this approximation and fixing $T_c = 5.4$ K (see the dashed line in the lower inset of Fig. 6), we obtain an isotropically averaged lower critical field of $\mu_0 H_{c1}(0) \approx 3.8$ mT. Depending on the criterion used for defining H_{c1}, these numbers may vary by a factor of unity [taking, for example, the maximum of $-m(H)$ as a criterion for H_{c1}, yields corresponding values that are larger by a factor of approximately 4]. Moreover, all these numbers represent again values that are averaged over all crystal directions. We can nevertheless state that these materials must be strongly type-II superconductors with a Ginzburg-Landau parameter of the order of $\kappa = \lambda/\xi \approx 35$ for $x = 0.2$, as estimated from the relations [21]

$$\mu_0 H_{c1} = \frac{\phi_0}{4\pi\lambda^2} \ln(\kappa + 0.5) \quad (5)$$

and

$$\frac{H_{c1}}{H_{c2}} = \frac{\ln(\kappa) + \frac{1}{2}}{\kappa^2}, \quad (6)$$

with a $\lambda \approx 4200$ Å.

IV. CONCLUSION

We have described the successful synthesis of the $Ba_{1-x}Rb_xTi_2Sb_2O$ ($x \leqslant 0.4$) solid solution, and presented data on their basic physical properties. X-ray diffraction data show that the compounds are single phase with a crystal structure isopointal to the $CeCr_2Si_2C$-type ($P4/mmm$) structure. Our temperature-dependent resistivity measurements reveal a continuous and drastic decrease of the CDW ordering transition temperature, by replacing barium by rubidium, with the CDW transition fully suppressed for $x \geqslant 0.2$. At this doping level, superconductivity reaches its maximum critical temperature $T_c = 5.4$ K (in specific-heat measurements). Both a well developed discontinuity in the specific heat at T_c and a large Meissner-shielding fraction indicate the bulk nature of superconductivity. A larger rubidium contents than the optimum value $x = 0.2$ leads to a decrease of the diamagnetic shielding fraction, with T_c remaining essentially unchanged. From our data we obtain estimates for the isotropically averaged lower and the upper critical fields $\mu_0 H_{c1}(0) \approx 3.8$ mT and $\mu_0 H_{c,2}(0) \approx 2.3$ T for the optimally doped sample with $x = 0.2$, indicating that these compounds are strongly type-II superconductors. Our results support the scenario that hole doping by the incorporation of Na^+, K^+, and also Rb^+ is of great importance for the suppression of CDW ordering and the occurrence of superconductivity in these materials.

ACKNOWLEDGMENTS

F.v.R. acknowledges support via a scholarship from Forschungskredit UZH, Grant No. 57161402. The authors would like to thank Michael Wörle for helpful discussions.

[1] J. Zhao *et al.*, Nat. Mater. **7**, 953 (2008).
[2] M. S. Torikachvili, S. L. Budko, N. Ni, and P. C. Canfield, Phys. Rev. Lett. **101**, 057006 (2008).
[3] D. E. Moncton, J. D. Axe, and F. J. DiSalvo, Phys. Rev. Lett. **34**, 734 (1975).
[4] L. F. Mattheiss and D. R. Hamann, Phys. Rev. Lett. **60**, 2681 (1988).
[5] D. E. Cox and A. W. Sleight, Solid State Commun. **19**, 969 (1976).
[6] E. Morosan, H. W. Zandbergen, B. S. Dennis, J. W. G. Bos, Y. Onose, T. Klimczuk, A. P. Ramirez, N. P. Ong, and R. J. Cava, Nat. Phys. **2**, 544 (2006).
[7] T. Wu, H. Mayaffre, S. Krmer, M. Horvatic, C. Berthier, W. N. Hardy, R. Liang, D. A. Bonn, and M. Julien, Nature (London) **477**, 191 (2011).
[8] T. Yajima, K. Nakano, F. Takeiri, T. Ono, Y. Hosokoshi, Y. Matsushita, J. Hester, Y. Kobayashi, and H. Kageyama, J. Phys. Soc. Jpn. **81**, 103706 (2012).
[9] P. Doan, M. Gooch, Z. Tang, B. Lorenz, A. Möller, P. C. W. Chu, and A. M. Guloy, J. Am. Chem. Soc. **134**, 16520 (2012).
[10] U. Pachmayr and D. Johrendt, Solid State Sciences **28**, 31 (2014).
[11] H.-F. Zhai, W.-H. Jiao, Y.-L. Sun, J.-K. Bao, H. Jiang, X.-J. Yang, Z.-T. Tang, Q. Tao, X.-F. Xu, Y.-K. Li, C. Cao, J.-H. Dai, Z.-A. Xu, and G.-H. Cao, Phys. Rev. B **87**, 100502(R) (2013).
[12] K. Nakano, T. Yajima, F. Takeiri, M. A. Green, J. Hester, Y. Kobayashi, and H. Kageyama, J. Phys. Soc. Jpn. **82**, 074707 (2013).
[13] S. Kitagawa, K. Ishida, K. Nakano, T. Yajima, and H. Kageyama, Phys. Rev. B **87**, 060510 (2013).
[14] F. von Rohr, A. Schilling, R. Nesper, C. Baines, and M. Bendele, Phys. Rev. B **88**, 140501(R) (2013).
[15] J. Rodriguez-Carvajal, Physica B **192**, 55 (1993).
[16] M. Gooch, P. Doan, Z. Tang, B. Lorenz, A. M. Guloy, and P. C. W. Chu, Phys. Rev. B **88**, 064510 (2013).
[17] N. R. Werthamer, E. Helfand, and P. C. Hohenberg, Phys. Rev. **147**, 295 (1966).
[18] V. G. Kogan and R. Prozorov, Rep. Prog. Phys. **75**, 114502 (2012).
[19] M. Naito, A. Matsuda, K. Kitazawa, S. Kambe, I. Tanaka, and H. Kojima, Phys. Rev. B **41**, 4823 (1990).
[20] C. P. Bean, Rev. Mod. Phys. **36**, 31 (1964).
[21] E. H. Brandt, Phys. Rev. B **68**, 054506 (2003).